Structural Hierarchy in Melt-Processed Poly(3-hexyl thiophene)−Montmorillonite Clay Nanocomposites: Novel Physical, Mechanical, Optical, and Conductivity Properties

Biplab K. Kuila and Arun K. Nandi*

Polymer Science Unit, Indian Association for the Cultivation of Science, Jadavpur, Kolkata 700 032, India

Received: September 15, 2005; In Final Form: November 26, 2005

Poly(3-hexyl thiophene) (P3HT) organically modified montmorillonite (om-MMT) polymer nanocomposites (PNCs) are prepared in the melt-cooled state. Hierarchical structures up to third order, namely, side chain mesomorph formation followed by the interchain lamellar structure of P3HT and finally its intercalation within the clay tactoids are observed. The structures are supported by transmission electron microscopy (TEM) and wide-angle X-ray scattering (WAXS) experiments. The TGA curves show two-stage degradation corresponding to those of the side chain and main chain of P3HT, and both temperatures decrease with an increase in clay concentration in the PNCs. The melting points of PNCs have increased by 2−3 °C higher than that of P3HT. The glass-transition temperature (T_g) and β-transition temperature (T_β), measured by DMA, increase with an increase in clay concentration. The storage modulus (G) of PNCs has also increased more dramatically than that of P3HT. The UV−vis spectra of the PNCs show a blue shift in the $\pi-\pi^*$ absorption peak of the conjugated chain, but the photoluminescence spectra showed a red shift with an increase in the clay concentration. The quantum yield of the photoluminescence process also increases in the melt-cooled PNCs, and this is in sharp contrast to that of solvent cast PNCs where photoluminescence quenching was observed. Fibrillar network structure of the solvent cast PNCs promotes energy transfer of the charge carriers, but its absence in the melt-cooled films inhibits such energy transfer, increasing the quantum yield. The room-temperature dc conductivity of the PNCs decreased by an order compared to that of P3HT in both the doped and undoped states. The $I-V$ characteristic curve shows semiconducting behavior, and it slowly transforms into insulator with increasing clay concentration.

Introduction

Recently, polymer clay nanocomposites (PNCs) have received significant attention because of the dramatic improvement in thermal, mechanical, and physical properties of the composite.[1−7] The large interfacial area and the nanoscopic dimensions of the clay tactoids are the possible factors for such a large scale improvement.[2] Apart from the study of polymer clay nanocomposites of commodity plastics, the conducting polymer clay nanocomposite are now studied significantly.[8−16] The aim of this research is not only to increase the mechanical properties as in commodity plastics but also to improve electronic, magnetic, and optoelectronic properties of these specialty polymers. Such PNCs, therefore, would produce materials for use in various sophisticated optical, electronic, and optoelectronic applications.

Among the conducting polymers, polyaniline and polypyrrole clay nanocomposites are the most widely studied.[10,12−16] Poly-(3-alkyl thiophenes) (P3ATs) are important members of these family for their solubility, functionality, conductivity, luminescence, and nonlinear optical properties.[17] In an earlier paper,[11] we focused on the preparation of PNCs of poly(3-hexyl thiophene) (P3HT) with organically modified montmorillonite (om-MMT) clay by the solvent cast method. Both 1% and 2.5% (w/w) clay content hybrid yielded exfoliated clay tactoids whereas the 5% clay content blend exhibited an intercalated clay structure. The storage modulus and thermal stability of these

PNCs increased dramatically whereas the conductivity remains the same. The absorption spectra showed a blue shift of the $\pi-\pi^*$ transition band of P3HT, and they showed photoluminescence quenching on excitation at a wavelength of 490 nm.

The p-type polymers, for example, poly(*p*-phenylenes), polyfluorenes, and polythiophenes usually exhibit photoluminescence with the holes as major carriers.[8] To improve the photoluminescence of these polymers, the insertion and confinement of carriers in a quantum well is necessary. Lee at al.[8] obtained enhancement of photoluminescence by making PNCs of poly-[2-methoxy-5-(2′-ethyl hexyloxy)-1,4-phenylene vinylene] (MEH-PPV) with om-MMT clay. Although poly(3-hexyl thiophene) has appreciable photoluminescence, in the solvent cast PNCs,[11] photoluminescence quenching was observed. In analogy with the MEH-PPV system,[8] the solvent cast PNC with 5% clay concentration should exhibit some enhancement in photoluminescence, but that was not observed. In the melt-cooled PNCs, however, enhancement in photoluminescence efficiency is observed at all clay concentration studied here. So it appears that some other internal and/or supramolecular structure of polythiophene is playing an important role in the photoluminescence property of the melt-cooled PNCs.

P3ATs are comblike polymers and produce an interchain lamellar structure in the solid state. Until now, three polymorphic structures of this polymer are reported.[18−20] Two are crystalline polymorphs, and the other is a mesomorph. The two crystalline polymorphs differ in the conformation and extent of interdigitation of the alkyl side chains. In the type-I crystal, the pendent alkyl groups are in staggered conformation and are tilted such

* To whom correspondence should be addressed. E-mail: psuakn@mahendra.iacs.res.in.

TABLE 1: Characteristics of the Samples

poly(3-hexyl thiophene) (P3HT)	montmorillonite clay[a] PGV; PV-178-00
product − synthesized	product − Nanocor, Inc. U.S.A.
H−T regioregularity = 82%	color − white
$\bar{M}_w$ = 111200	cation exchange
PDI = 1.78	capacity (mequiv/100 g) = 101.4[b]
melting point = 189 °C	aspect ratio = 150−200
	specific gravity = 2.6

[a] Data from Nanocor, Inc. [b] Measured value using TGA.[11]

that they remain in the hexagonal close packed structure. The overlapping of the side chains is minimal, but the ordering of the side chain exists across the layer-to-layer interface. In the planar type-II crystal, the interdigitation of the side chains occurs, fully reducing the interchain lamellar thickness by ∼30% compared with the type-I crystals. Type-I crystals are produced by casting the P3AT solutions rapidly at high temperature, whereas slow casting of the P3HT solution at room temperature produces type-II crystals. Upon modest heating, the type-II crystal undergoes a solid-state transformation to type-I crystal, which is the most stable polymorph. Upon further heating, the type-I crystal transforms into mesomorphic structure. The melt on slow cooling also produces the same. This phase is characterized by a broad X-ray peak at $2\theta \sim 20°$ together with the interchain lamellar spacing of type-I crystal.[20]

In the PNCs produced by solvent cast method, the formation of type-I crystals of P3HT is reported. The interchain lamella of type-I crystals was produced from the side chain crystallization of P3HT. The variation of side chain structure is possible, for example, it may be planar, in mesomorphic arrangement, etc. This difference in arrangement, that is, change in hierarchical structure might cause different properties in these important PNCs. In this article, we want to explore the effect of different hierarchy on the physical, mechanical, optical, and conductivity properties of the PNCs. Also the effect of a different supramolecular structure of the whole system produced from a different preparation procedure of the PNCs will be discussed. Such a study would help technologists to obtain tailor-made products of different physical, mechanical, and optical properties by tuning preparation method, samples, etc.

Experimental Section

a. Samples. P3HT (regioirregular) was synthesized from the monomer 3-hexyl thiophene in chloroform using anhydrous $FeCl_3$ as the initiator under a nitrogen atmosphere at 0 °C for 24 h.[21] The reaction mixture was poured into methanol containing 10% (12 N) HCl, and the precipitate was washed with methanol. It was then dissolved in chloroform, filtered from impurities, and dried to get the P3HT film. The head−tail (H−T) regioregularity of the sample was measured from ^{1}H NMR spectra in $CDCl_3$,[15] and the molecular weight ($\bar{M}_w$) of the samples was measured from gel permeation chromatography (G.P.C., Waters) using $CHCl_3$ as the solvent and polystyrene as the standard. The MMT clay (PGV-PV-178-00, Nanocor, Arlington Height, IL) was organically modified using cetyl trimethylammonium bromide (CTAB).[11,22] The exchange capacity of the clay was measured using thermogravimetric analysis, and it was found to be 101.4 mequiv/100 g (equivalent wt of CTA ion 288). The characteristics of the samples are presented in Table 1.

b. Preparation of the Nanocomposite. The PNCs were first prepared by the solvent cast method as reported earlier[11] using chloroform as the medium. The dried films were melted at a

Metler hot stage at 210 °C for 10 min and were then cooled to 30 °C under nitrogen atmosphere by switching off the hot stage. This process was repeated for two times to ensure complete melt mixing. These melt-cooled samples were then characterized, and physical properties were measured. The nanocomposites are designated as PNC1, PNC2.5, and PNC5, the number at the right-hand side indicates the clay percentage (w/w) in the composite.

c. Wide-Angle X-ray Scattering (WAXS) Study. The WAXS data were taken from the above melt-cooled films by a Seifert X-ray diffractometer model (C 300) in reflection mode with a parallel beam optics attachment. Nickel-filtered copper K_α radiation ($\lambda = 0.154$ nm) operating at a 35 kv voltage and a 30 mA current was used. The samples were scanned from $2\theta = 2°$ to 45° at the step scan mode (step size, 0.03°, preset time, 2 s), and the diffraction pattern was recorded using a scintillation counter detector.

d. Transmission Electron Microscopy (TEM). The morphology of the PNCs was studied using a JEOL high-resolution electron microscope (model 2010EX) operated at an accelerated voltage of 200 kV without staining. A CCD camera was used to take the picture. The PNCs were encapsulated in epoxy matrixes and then sectioned into thin sections (thickness ∼70 nm) at 25 °C by a ultracryomicrotome (Ultra R, Leica) equipped with glass knife. It was placed on a copper grid and was observed through the microscope.

An SEM study of the melt-cooled and solvent cast PNCs was made using a scanning electron microscope (JEOL GSM-5800). The samples were gold coated prior observation.

e. Thermal Measurement. The thermal stability of the PNCs was measured using a Metler Toledo TGA (SDTA 851e) instrument under N_2 atmosphere at a heating rate of 10°/min. For the differential scanning calorimetry (DSC) experiment, a Perkin-Elmer DSC-7 fitted with intracooler-1 and working under a nitrogen atmosphere was used in this work. It was calibrated with indium before each set of experiment. The melt-cooled samples (∼3 mg) in aluminum pans were heated at the heating rate of 10 °C/min from −30 to 210 °C under N_2 atmosphere. From the endothermic peak, the melting point and enthalpy of fusion were measured, using pc-series DSC-7 multitasking software (version 3.2).

f. Spectral Characterization. The FTIR spectra of the samples were performed from the films in a Nicolet FTIR instrument [Magna-1R-750 spectrometer (series-11)]. The UV−vis spectra of the PNCs were studied by melting the solvent cast films on quartz plates at 210 °C under N_2 atmosphere in a Metler FP-82 hot stage and then cooled to 30 °C by switching off the hot stage. It takes about 30 min to cool the melt from 210 to 30 °C. The spectra were taken against air at 30 °C in a UV−vis spectrophotometer (Hewlett-Packard, model 8453) from 200 to 1000 nm. The photoluminescence experiments of the melt-cooled films were performed in a Perkin-Elmer instrument (LS55 Luminescence spectrometer). The photoexcitation was made at an excitation wavelength of 500 nm at a 45° angle of the thin film plane. The emission was detected at a right angle to the excitation beam direction. Each spectrum was normalized with the film thickness of 1 μm for comparison purposes.

g. Dynamical Mechanical Property Measurements. The storage modulus (G), loss modulus (G'), and tan δ of the PNCs were measured using a dynamic mechanical analyzer (DMA) (TA instruments model Q-800). Films of 25 mm × 5 mm × 0.15 mm dimensions were cast from the composite solutions on a die. Then they were melted twice in a Metler hot stage at

Poly(3-hexyl thiophene)−Montmorillonite

J. Phys. Chem. B, Vol. 110, No. 4, 2006 **1623**
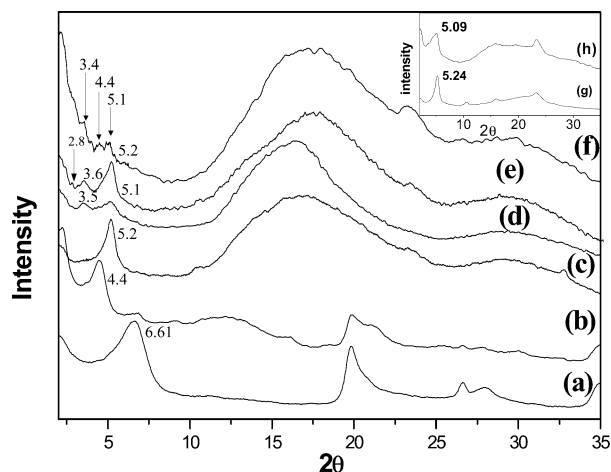
Figure 1. WAXS patterns of melt-cooled om-MMT−P3HT nanocomposites (a) pure clay, (b) om-clay, (c) P3HT, (d) PNC1, (e) PNC2.5, and (f) PNC5 (inset, solvent cast samples of (g) P3HT and (h) PNC5).

210 °C for 10 min and then cooled to 30 °C in the hot stage. These films were then installed in the tension clamp of the calibrated instrument. The sample was heated from −130 to 100 °C at the heating rate of 10 °C/min. The storage modulus (G), loss modulus (G'), and tan δ were measured at a constant frequency of 1 Hz with a static force of 0.02 N.

h. dc Conductivity Measurement. The dc conductivity of a PNC film at 30 °C was measured by the standard spring-loaded, pressure-contact, four-probe method.[23] A circular film of 1−3 cm diameter was used, and the probes were connected with the help of an Ag paste. A constant current (I) was passed from a dc source electrometer (Keithley model 617) through two diagonal leads of the four probes, and the voltage (V) across the other two leads was measured using a multimeter (Keithley, model 2000). The conductivity (σ) was calculated from the relation

$$\sigma = (\ln 2/\pi d)(I/V) \tag{1}$$

Where d, the thickness of the film was taken as the average of four measurements at different places using a screw gauge. Conductivities of two films each with two trials were measured, and the average of four such measurements was taken as the conductivity of the samples. The conductivity of the doped samples was measured by exposing the films in iodine vapor for 24 h. The $I−V$ characteristic curves of the samples were measured by gold coating both sides of the central portion of the film and then connecting through two copper wires with silver paste.

Results and Discussion

A. WAXD and TEM. In Figure 1, the WAXS diffraction patterns of the melt-cooled films of PNCs are presented. It is apparent from the figure that pure P3HT has a lamellar peak at $2\theta = 5.2°$ (lamellar thickness = 17.1 Å) and an amorphous halo at $2\theta \approx 17°$. This halo is present in all the PNCs studied together with two lamellar peaks at 2θ values ~3.5° and ~5.1°. The organically modified clay has one lamellar peak at $2\theta = 4.4°$ (lamellar thickness = 20.1 Å), but in the PNC1 and PNC2.5, this peak is shifted to $2\theta = 3.5°$. This shift of clay lamella to a lower angle indicates that some polymer chains are intercalated within the clay lamella. In PNC2.5, another peak at $2\theta = 2.8°$ is observed corresponding to a lamellar thickness of 32 Å. The amorphous halo at $2\theta = 17°$ together with the lamellar peak corresponds to the liquid crystalline polymorph

of P3HT.[19,20] Thus, it may be surmised that a liquid crystalline intercalated lamellar structure is produced in the melt-cooled PNCs, and this is in sharp contrast to the PNCs produced by the solvent cast method where a type-1 crystalline polymorph was produced (see inset of Figure 1).[11] In parts a−d of Figure 2, the TEM micrographs of the melt-cooled PNCs are presented. Each micrograph characterizes the formation of intercalated lamellar structured nanocomposites where P3HT chains/lamella remain intercalated within the clay tactoids. In micrograph 2e (Figure 2), the morphology of the solvent cast PNC2.5 sample is compared with that of the melt-cooled samples. It is apparent from the figure that the clay tactoids are not parallel to each other, rather they are in angular dispositions with an average distance larger than 10 nm between them. This characterizes the exfoliated morphology in the solvent cast samples. It may therefore be concluded that the morphology of melt-cooled samples is different from the solvent cast samples.

In the present case, three possibilities exist according to Scheme 1: (i) single P3HT chain intercalation between the om-clay tactoids, (ii) a P3HT lamella (i.e., two interdigited chains) may remain intercalated, and (iii) multiple P3HT lamellas may also remain intercalated. This can be easily judged from the X-ray spacings at the lower angles. In the present result (Figure 1), the diffraction peak at $2\theta = 3.5°$ corresponds to lamellar spacing 25.5 Å, which is 5.4 Å larger than the spacing of the tactoids of om-clay (20.1 Å). A single P3HT chain may therefore be accommodated between the organoclay tactoids as shown in Scheme 1b. (The molecular thickness of the thiophene unit is 2.6 Å and that of the hexyl group is 7.4 Å as obtained from molecular mechanics (MMX) program.[24] So there would be an interdigitation of 6 Å for each hexyl group of P3HT.) The lamella peak at $2\theta = 2.8°$ corresponds to a lamellar distance of 31.5 Å which is 11.4 Å larger than that of clay lamella. The lamella distance of P3HT lamella is 17.1 Å; so within the experimental uncertainty of the results, it may be proposed that P3HT lamella had to be squeezed to some extent to intercalate into clay lamella. Also, the interdigitation of the cetyl groups of om-clay and hexyl groups of P3HT might be possible to a large extent. This is represented in Scheme 1c. The cetyl groups are anchored from the clay tactoids, and due to the same hydrocarbon nature, the interdigitation between hexyl and cetyl groups is possible to a very large extent. The strong cohesive force of attraction between the clay tactoids forming the sandwiched structure might be the reason for such a large interdigitation. Arrangements such as Scheme 1d (two P3HT lamella intercalations) are also possible, but due to the limitation of our X-ray instrument, we could not afford any evidence. In a word, the intercalated structure is polydisperse in nature.

Of particular interest, what is the arrangement of side chains or the intercalated chains with om-clay tactoids? The wide halo at 17° in all PNCs clearly supports that they are all in mesomorphic arrangement. This is in sharp contrast to the solvent cast PNCs where they produce a type-I crystal (inset of Figure 1). During the melt-cooling process, the cooling rate (by switching off the Metler hot stage) is slow and the presence of clay tactoids also inhibits the heat dissipation, making the cooling rate even more slow. In this condition, liquid crystalline polymorph formation of poly(3-alkyl thiophene) (P3AT) is reported.[19,20] In Scheme 1, the arrangement of the side chains of P3HT is elaborated together with the cetyl group of CTAB. The arrangement might be considered as schematic-type liquid crystal. Further, the arrangement of the hexyl and cetyl chains
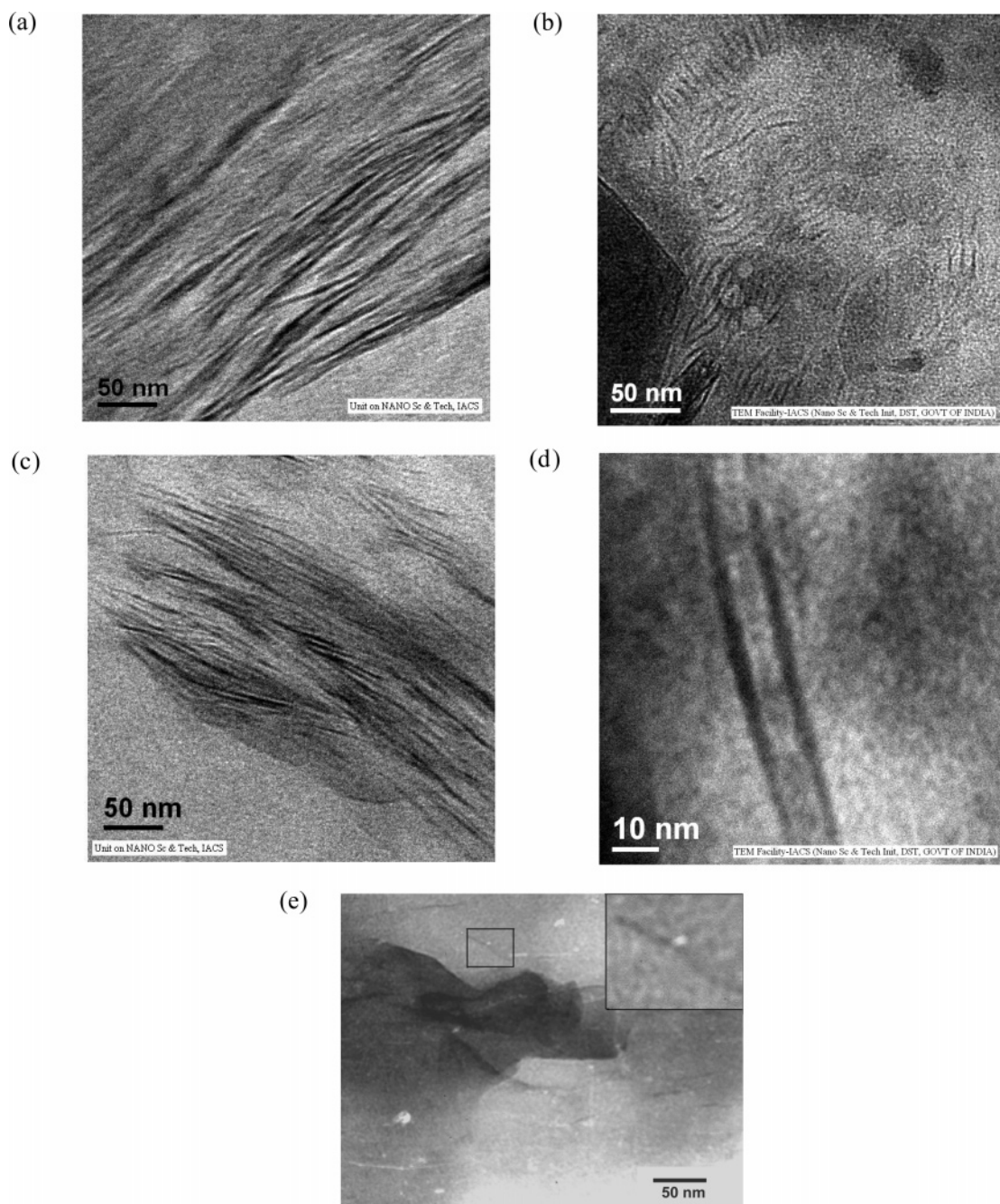
Figure 2. TEM micrographs of melt-cooled om-MMT−P3HT nanocomposites (a) PNC1, (b) PNC2.5, (c) PNC5, (d) enlarged portion of PNC1, and (e) solvent cast PNC2.5 (inset, enlargement of box mark).
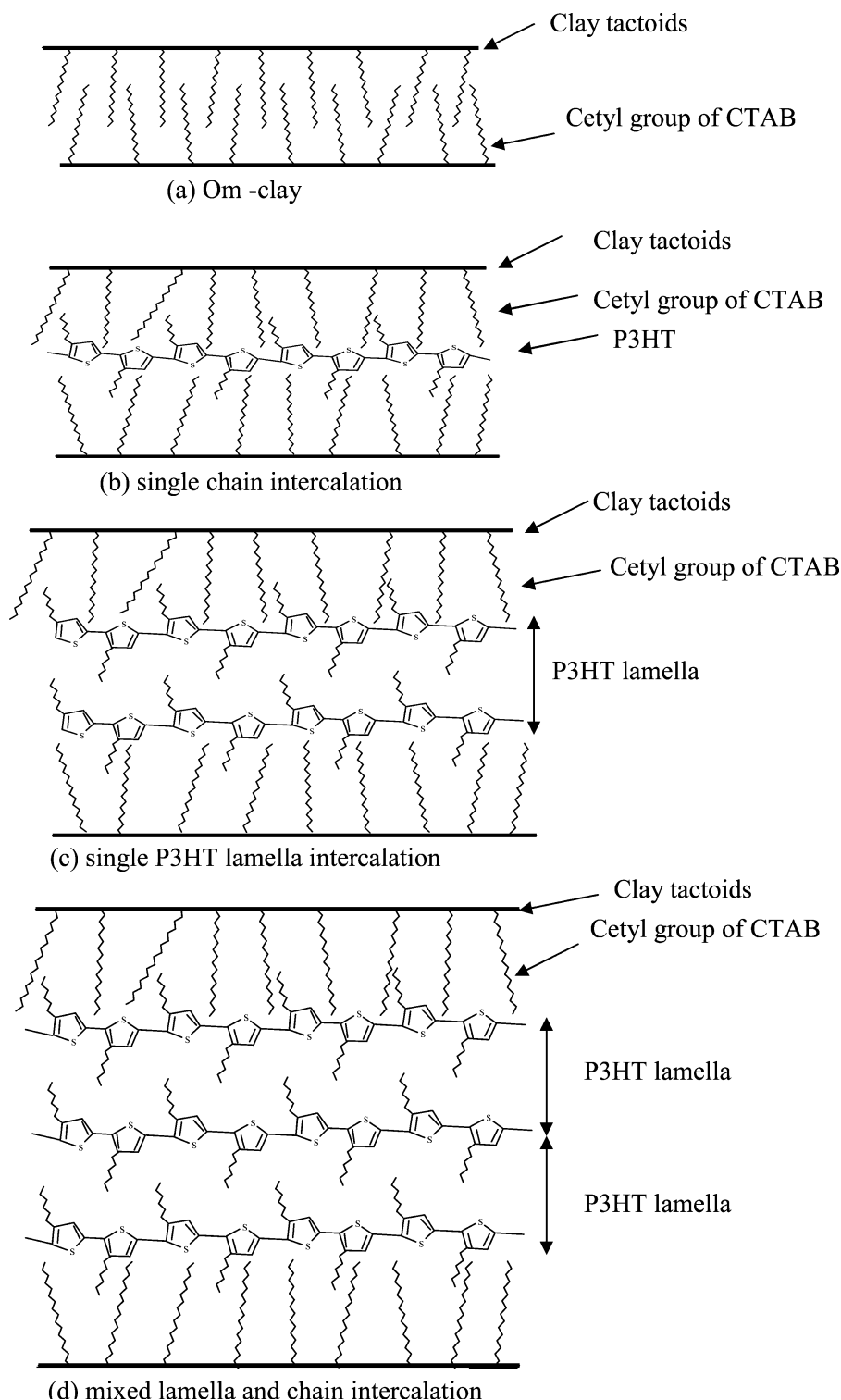
may not be what is actually presented here, and some more disorderliness by bending and folding of the side chains is quite natural.

B. FTIR Spectra. The FTIR spectra of the melt-cooled PNCs and om-MMT are presented in Figure 3. The om-MMT has peaks at 3623, 2923, 2851, 1663, 1474, 1032, 518, and 462 cm^{-1}. The 3623 cm^{-1} peak is for the absorption band of lattice water (O−H stretching),[26] while the peaks at 2923, 2851, and 1474 cm^{-1} are for CH$_2$ asymmetric stretching, symmetric stretching, and in-plane scissoring vibrations, respectively. The 1663 cm^{-1} peak may be attributed to H−OH bending of the lattice water. The P3HT has absorption peaks at 3055 cm^{-1}, for aromatic CH stretching, 2916 cm^{-1} for asymmetric CH$_2$ stretching, and 2857 cm^{-1} for symmetric CH$_2$ stretching. The 1512 and 1460 cm^{-1} peaks of P3HT characterize the ring stretching, and the 1377 cm^{-1} peak is for methyl deformation.

The 827 cm^{-1} peak of P3HT is for aromatic CH out-of-plane vibration, and the 726 cm^{-1} peak is for methyl rocking.[26] In the PNCs, the characteristic peaks of the om-clay are retained, and its intensity increases with the increasing concentration of the om-clay. The Si−O−Si band at 1032 cm^{-1} of the om-clay shifts to higher energy, for example, 1035 cm^{-1} for PNC1, 1034 cm^{-1} for PNC2.5, and 1040 cm^{-1} for PNC5 because of the intercalation of the P3HT chain into the clay lamella making it more compact. Due to the increased compactness of clay tactoids, the Si−O−Si vibration requires higher energy.

C. Thermogravimetric Analysis. The TGA thermograms of the melt-cooled PNCs are presented in Figure 4. It is apparent from the figure that the melt-cooled PNCs have lesser stability than that of pure P3HT. In contrast, the solvent cast PNCs showed an increase in thermal stability[11] as presented in the inset of Figure 4. There are two degradation temperatures in

SCHEME 1. Schematic Models of the Intercalated Structure of P3HT PNCs

(a) Om -clay

(b) single chain intercalation

(c) single P3HT lamella intercalation

(d) mixed lamella and chain intercalation

the present system, and they are plotted in Figure 5 with clay concentration. A decrease in both the degradation temperatures with increasing clay content is observed. Also the residue left at 800 °C is higher for P3HT than for PNCs. The enhancement of thermal stability is common in the PNCs[11,22] but a decrease in thermal stability of PNCs is also reported by others.[27] This difference in thermal stability between solvent cast and melt-cooled PNCs may be due to the structural difference of solvent cast and melt-cooled films. Probably, the two-stage degradation arises from the degradation of the side chains and degradation of the main chain of P3HT, respectively. The former occurs at
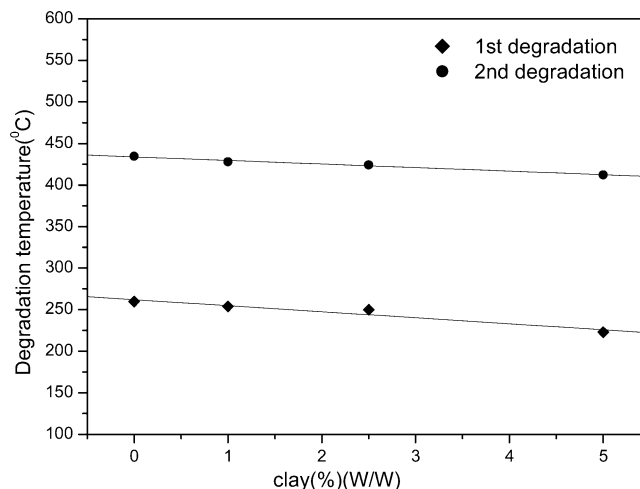
a lower temperature, for example, around ∼250 °C, whereas the latter occurs at around 430 °C. This seems to be reasonable as aliphatic chains are easily attacked by oxygen at a lower temperature. The heterocyclic ring and the conjugation of the chain make the main chain more stable. The effect of clay concentration on the relative degree of degradation in the side chain and in the main chains might be considered from the least-squares slope of the degradation temperature vs clay concentration plots shown in Figure 5. The least-squares slope value of first degradation is −7.2 while that of the second degradation is −4.2, that is, the rate of degradation of the pendent alkyl
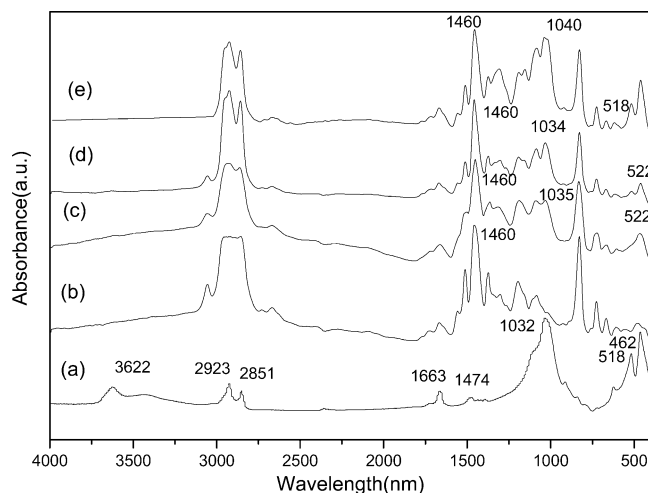
Figure 3. FTIR spectra of melt-cooled PNCs (a) om-MMT, (b) P3HT, (c) PNC1, (d) PNC2.5, and (e) PNC5.

Figure 5. Plot of degradation temperature vs clay content for the two-stage degradation process of the melt-cooled PNCs.

group is approximately two times faster than that of the thiophene main chain in the presence of clay. It is therefore reasonable to think that the presence of clay is deteriorating the ordered state of the side chains more when compared to the main chain, causing the former to degrade at a faster rate with the increase in clay concentration. In our earlier report, it was shown that the solvent cast PNCs have type-I crystals and their degradation temperature has increased significantly. So it may be surmised that the melt-cooled films have a different structure than the solvent cast samples, and X-ray evidence clearly indicates that the side chains are in mesomorphic form. Due to this mesomorphic nature of the side chains, the melt-cooled PNCs degrade more rapidly than the solvent cast samples.

D. Diffential Scanning Calorimetry (DSC). In Figure 6, the DSC thermograms of melt-cooled PNCs are presented, and in the inset, the typical DSC thermograms of solvent cast

samples are also compared. The main chain melting peaks are clearly observed at the temperature range (183−186 °C), but the side chain melting peaks, which usually occur at ∼50 °C,[28] are not at all observed. Generally, the side chain melting peak in P3HT occurs at samples having head tail regioregularity ≥90 mol %. It might be probable that the lower H−T regioregularity in the sample promotes the side chain as liquid crystalline. Also, the molecular weight of the poly(3-alkyl thiophene) has a strong influence on the crystalline polymorph (type-I, type-II) and mesomorph formation.[19,20] The melting points of melt-cooled P3HT are 182.9, 185.1, 185.8, and 186.2 °C, respectively, and they are 7−14 °C lower than those of the solvent cast films[11] (cf. inset of Figure 6). It is really interesting, and it also supports that the solvent cast PNCs are of different structure than the melt-cooled films.[28] The lower melting points in the melt-cooled samples reflect that they are more disordered than the solvent
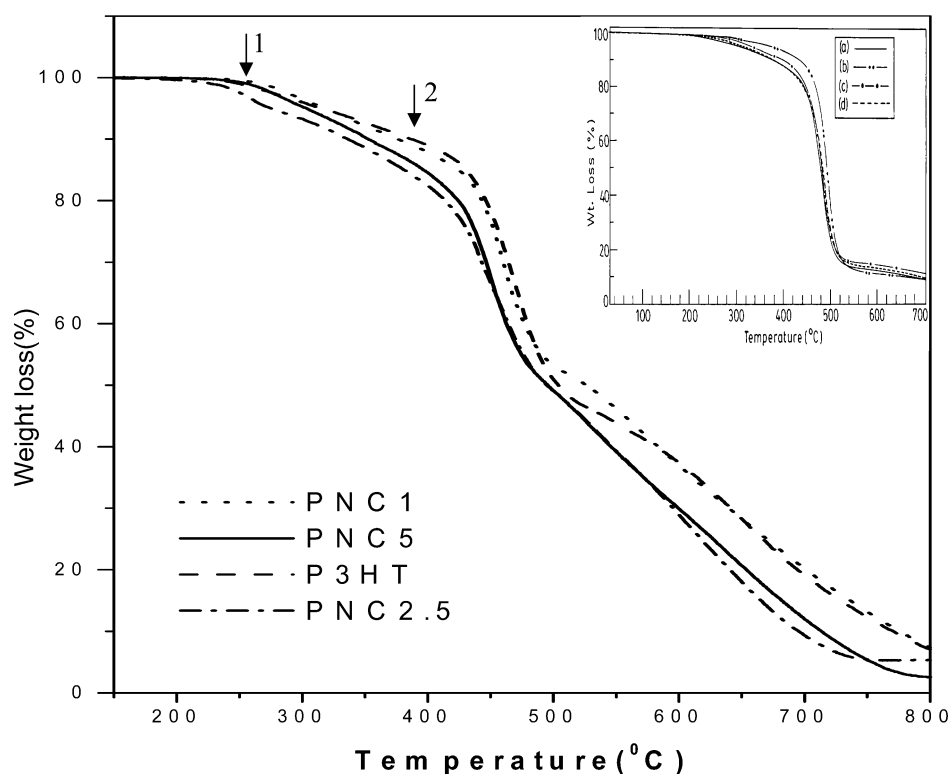
Figure 4. TGA thermograms of melt-cooled PNCs under N$_2$ atmosphere at 10 °C/min heating rate (inset, TGA thermograms of solvent cast PNCs: (a) P3HT, (b) PNC1, (c) PNC2.5, and (d) PNC5).

Poly(3-hexyl thiophene)−Montmorillonite

J. Phys. Chem. B, Vol. 110, No. 4, 2006 **1627**
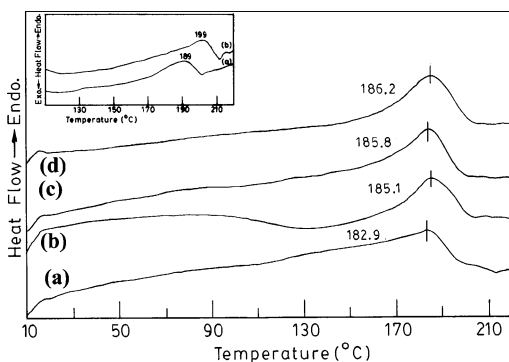
Figure 6. DSC thermograms of the melt-cooled P3HT PNCs: (a) P3HT, (b) PNC1, (c) PNC2.5, and (d) PNC5 (inset, for solvent cast samples (a) P3HT and (b) PNC1).

cast films, and probably, the crystallization/ordering of the side chains in the solvent cast film induces P3HT main chains to crystallize more perfectly than the melt-cooled films. The enthalpy of fusion values are 6.7, 5.7, 5.6, and 6.1 J/g

for melt-cooled samples of P3HT, PNC1, PNC2.5, and PNC5, respectively. The results indicate that within experimental uncertainty the main chain ordering is not affected much due to intercalation of P3HT lamella into clay lamella. It is interesting to know the factor that increased the melting point of the PNCs by 2−3 °C from that of pure P3HT. No definite reason is known, and it might be probable that the P3HT chains/lamellas become straightened or extended within the clay lamella and this extension of the chain produces a higher melting point of the main chain crystal of P3HT in the melt-cooled PNCs.[29] The higher melting point of solvent cast PNCs compared to the melt-cooled samples is due to the more ordered type-1 crystallite formation in the former case.

E. Mechanical Properties. The storage modulus, loss modulus, and tan δ plots of PNCs prepared at the melt-cooled state are presented in Figure 7. From the plot (Figure 7a), it is apparent that the storage modulus of PNCs gradually increases at each temperature with increasing clay concentration. In the inset of Figure 7a, the storage modulus' of solvent cast films are presented and they are very similar in nature to the melt-cooled PNCs. With an increase in temperature, the storage modulus decreases at each case, however, the storage modulus does not decrease linearly. It may be better represented by two breaks, one around −100 °C and the other around 25 °C. These two breaks are better observed in the loss modulus vs temperature plot (Figure 7b) where it shows two peaks in each sample. The low-temperature peak may be termed as a β-transition temperature (T_β), and the higher temperature peak may be termed as a glass-transition temperature (T_g).[11,30] The T_β and T_g values are presented in Table 2, and it is clear from the table that both the T_g and T_β values increase with increasing clay concentration. The T_β increases by 3−13 °C and the T_g increases by 11−16 °C in the PNCs depending on the clay concentration. In Table 2, also, the T_g and T_β values of solvent cast PNCs are presented for comparison. Both the T_g and T_β values of melt-cooled samples are higher than those of the solvent cast samples. In Figure 7c, the tan δ plots of all PNCs are presented and here only the higher temperature peak is observed. The peak temperatures are about 20 °C higher than the loss modulus peak temperatures. The reason is yet not known to us.

Now, it is a reasonable question why both T_g and T_β increase in the PNCs. The T_β arises from relaxation of the side chain and the T_g arises from the relaxation of the main chain. All the PNCs have intercalated structure, the P3HT chains (both side chain and main chain) therefore experience restriction in

movement due to the compactness of the intercalated structure. Also, the cohesive force between the clay tactoids makes the composite more rigid. Consequently, a higher temperature is necessary for the commencement of the segmental Brownian motion of both the side chain and main chain yielding higher T_β and T_g values. The lower values of T_β and T_g of solvent cast films than melt-cooled films will be discussed now. In the solvent cast films, the free volume of P3HT is much higher than that of melt-cooled films and it may be possible as removal of solvent molecules creates some voids in the P3HT matrix. As a result, at a lower temperature, the system attains the free volume fraction 0.025 required for glass transition.[31,32] On the other hand, solvent-created free volumes are absent in the melt-cooled films. So a higher temperature is necessary to attain the free volume fraction 0.025 for the glass transition[31,32] and it is true for all the melt-cooled PNCs.

The mechanical reinforcement of the clay in the PNCs can be visualized well from the storage modulus data in Table 2 where the storage modulus (G) of P3HT and PNCs is presented for different temperatures. There is an increase in both G values, and its percentage increases with an increase in clay concentration. Though the G values decrease with an increase in temperature, the percentage increase of G increases with an increase in temperature for a particular clay concentration (Table 2). At −50 °C, the samples are in glassy form and here polymer chains do not have any movement except the side chain movement. So the reinforcement effect of clay tactoids is lesser. With an increase in temperature, the chains become less compact and as a result the reinforcement effect increases. Above the glass transition temperature (T_g), the polymer is in the rubbery state and the motion of chain segments is relatively free. At this temperature (see data of 50 °C), the reinforcement effect of clay nanoparticle is very large causing maximum reinforcement. The maximum reinforcement occurred here is 387%, however it is lesser than the maximum reinforcement (773%) obtained in solvent cast samples.[11] The reason for such a large difference between the two types of PNCs in reinforcement by clay tactoids may be explained from the fact that the solvent cast films have more free volumes than those in the melt-cooled films. The segmental motion of the chains in the former case is larger due to the larger free space, and as a result, the reinforcement effect by clay tactoids is larger than that by melt-cooled films. However, the effect of the different microstructure of the side chain and the overall supramolecular structure of the PNCs on the mechanical properties of the two types of samples cannot be completely ruled out.

F. UV−Vis Spectra. In Figure 8, the UV−vis spectra of the melt-quenched PNCs are presented. In each spectra, there is a hump at 272 nm corresponding to a $\pi-\pi^*$ transition of the thiophene ring. A peak at ~506 nm for pure P3HT corresponds to a $\pi-\pi^*$ transition of the conjugated chain.[33] However, in the PNCs, there is a blue shift of ~20 nm from pure P3HT for the $\pi-\pi^*$ transition of the conjugated chain. Here, it is noteworthy that there is a blue shift of the main peak of melt-cooled P3HT by 10 nm from that of the solvent cast P3HT films (cf. inset of the figure).[11] In the case of PNCs, the above shifts are ~20 nm. The reason may be due to the fact that in the solvent cast samples the P3HT chains remain more straight than in the melt-cooled films where the chains become more coiled and also entangled. As a result, the conjugation length of the melt-cooled chains is lower than that of the solvent cast films causing a blue shift in the UV−vis spectra. In the melt-cooled PNCs, such as the solvent cast PNCs, there is a blue shift of the main absorption peak from that of pure P3HT with

(a)

(b)

(c)
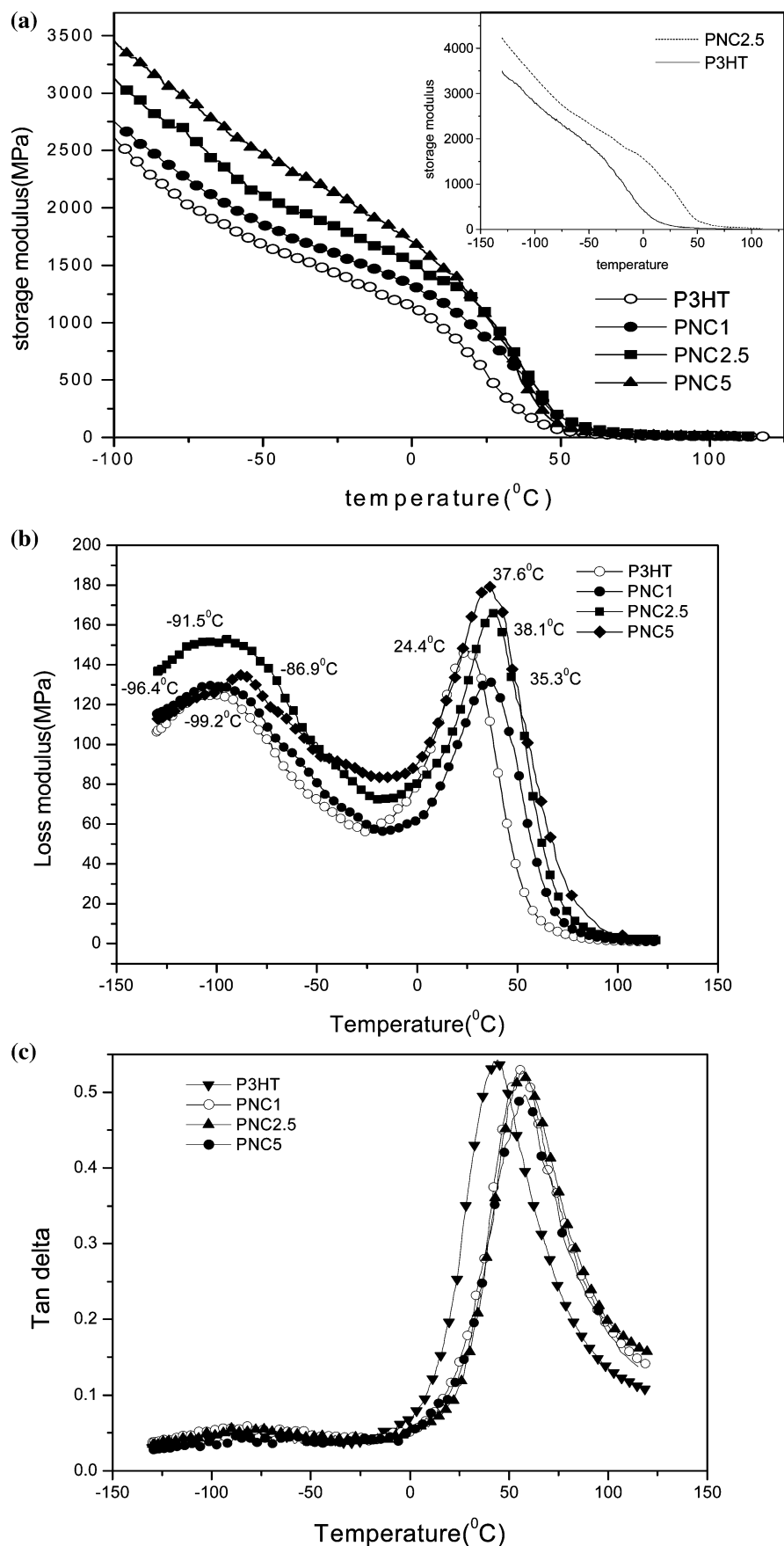
Figure 7. Mechanical property variation of melt-cooled P3HT nanocomposites with temperature: (a) storage modulus (inset, solvent cast samples), (b) loss modulus, and (c) tan δ.

increasing clay concentration. A similar blue shift in the UV−vis spectra was also observed in CdS-embedded P3HT nano-wire.[34] The degree of the blue shift is lower in the solvent cast than in the melt-cooled PNCs. The cause of such a blue shift is

Poly(3-hexyl thiophene)−Montmorillonite

J. Phys. Chem. B, Vol. 110, No. 4, 2006 **1629**

TABLE 2: Summary of Mechanical Properties of PNCs Measured by DMA

	T_β (°C)[a]		T_g (°C)[a]		storage modulus (MPa) at					
sample	solvent cast	melt quenched	solvent cast	melt quenched	−50 °C	(%) increase	20 °C	(%) increase	+50 °C	(%) increase
P3HT	−102.1	−99.2	−16.0	24.4	1681		706		64	
PNC1	−97.8	−96.4	25.2	35.3	1850	10	999	41.50	187	192
PNC2.5	−98.3	−91.5	28.2	38.1	2146	27.6	1259	78.3	232	262.5
PNC5	−84.6	−86.9	31.7	37.6	2515	49.6	1335	89	312	387.5

[a] From loss modulus peaks.

TABLE 3: Conductivity Values σ (S/cm) of Undoped and I$_2$-Doped P3HT and It's PNCs

	undoped		doped	
sample	solvent cast	melt quenched	solvent cast	melt quenched
P3HT	6.7×10^{-5}	2.6×10^{-4}	0.34	2.4×10^{-2}
PNC1	1.2×10^{-4}	4.6×10^{-5}	1.15	3.3×10^{-3}
PNC2.5	7.2×10^{-5}	3.9×10^{-5}	1.09	8.8×10^{-3}
PNC 5	7.5×10^{-5}	5.0×10^{-5}	1.04	4.3×10^{-3}

induced rigidity by clay tactoids.[35] As T_g is increasing with clay content due to the cohesive force between clay tactoids, it may produce kink and entanglement in the chains. This shortens the conjugation length of the main chain and causes the blue shift of the UV−vis absorption spectra. The larger blue shift in the melt-cooled PNCs from pure P3HT compared to that of solvent cast PNCs is due to the more coiled and entangled structure of P3HT chains in the melt-cooled state as stated above.

G. Photoluminescence Spectra. Figure 9 shows the photoluminescence spectra of the melt-cooled P3HT and its PNCs, and these spectra are different from those of the solvent cast samples (see inset of Figure 9).[11] In the latter system, there was photoluminescence quenching with increasing clay concentration, but the melt-cooled PNCs clearly exhibit an increase in photoluminescence efficiency with increasing clay concentration (Figure 9). This is really interesting as an opposite effect is observed in the samples prepared in the two different procedures. The reason for such an opposite phenomenon may arise from the change in structural hierarchy or any morphological effect. As suggested from the above results, here the hexyl side chains are in the mesomorphic state but in the solvent cast samples they were in the type-I crystalline state with a hexagonal close packed structure. Scheme 1 illustrates the structure of the melt-cooled PNCs. Due to the mesomorphic nature of the hexyl side chains, P3HT exhibits diminished normalized photoluminescence intensity by eight times (cf. inset of the figure). It might be probable that a liquid crystalline polymorph has a long-range disorder, and this may be a reason for the decreased photoluminescence efficiency of P3HT.

Now, the cause of photoluminescence intensity enhancement and the red shift of the melt-cooled PNCs in the present system will be discussed. In the intercalated state, the P3HT chains exist between the clay tactoids as single chain or as interchain lamella or a mixture of the two (Scheme 1). As a result, the interchain Froster energy transfer is difficult, instead intrachain energy transfer would increase.[36] So the higher energy excitons would migrate into a lower energy state along the same chain causing photoluminescence intensity enhancement. The red shift of photoluminescence spectra of the melt-cooled PNCs with clay concentration is comparable to that of poly(2-methoxy-5-(2′-ethoxyloxy)-1,4-phynelene vinylene)(MEPPV)/toluene systems[37] and oriented dendritic side group phenylene vinylene polymer.[38] This is usually called a red edge effect, and it arises due to the structural polydispersity of the luminating medium. In this system, various types of intercalated structures are present with increasing clay concentration as exemplified in Scheme 1. As a result, the red shift of the luminescence spectra is observed.
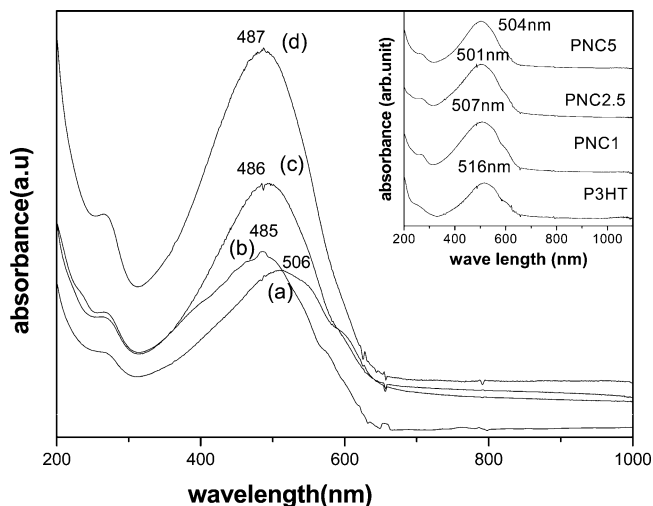
Figure 8. UV−vis absorption spectra of melt-cooled PNCs: (a) P3HT, (b) PNC1, (c) PNC2.5, and (d) PNC5 in the solid state at 30 °C (inset, solvent cast PNCs).
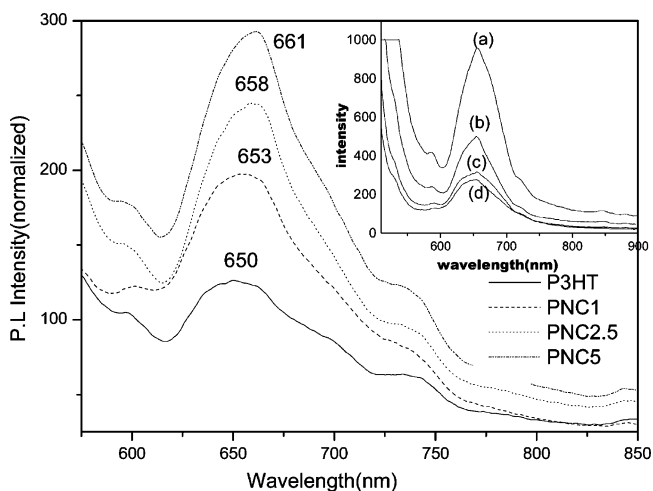
Figure 9. Photoluminescence spectra of melt-cooled P3HT and the PNCs after excitation by radiation of 500 nm wavelength (normalized to film thickness of 1 μm): (a) P3HT, (b) PNC1, (c) PNC2.5, and (d) PNC5 (inset, solvent cast PNCs (a) P3HT, (b) PNC1, (c) PNC2.5, and (d) PNC5).

The enhancement of photoluminescence efficiency may be explained by two factors: (i) the reduced interchain interaction as the intercalated clay lamella prevents excitons to find low-energy trap sites and (ii) an increased excitation beam path that occurs from internal scattering or reflection within the intercalated clay tactoids.[8,36] Due to these causes, photoluminescence efficiency is increased.

The cause of difference in behavior of solvent cast and melt-cooled PNCs will now be illustrated here. In Figure 10, the SEM micrographs of solvent cast and melt-cooled films are presented. It is apparent from the figure that the solvent cast samples have a fibrillar network structure but in the melt-cooled samples this is absent. The network structure is responsible for

(a)

(b)
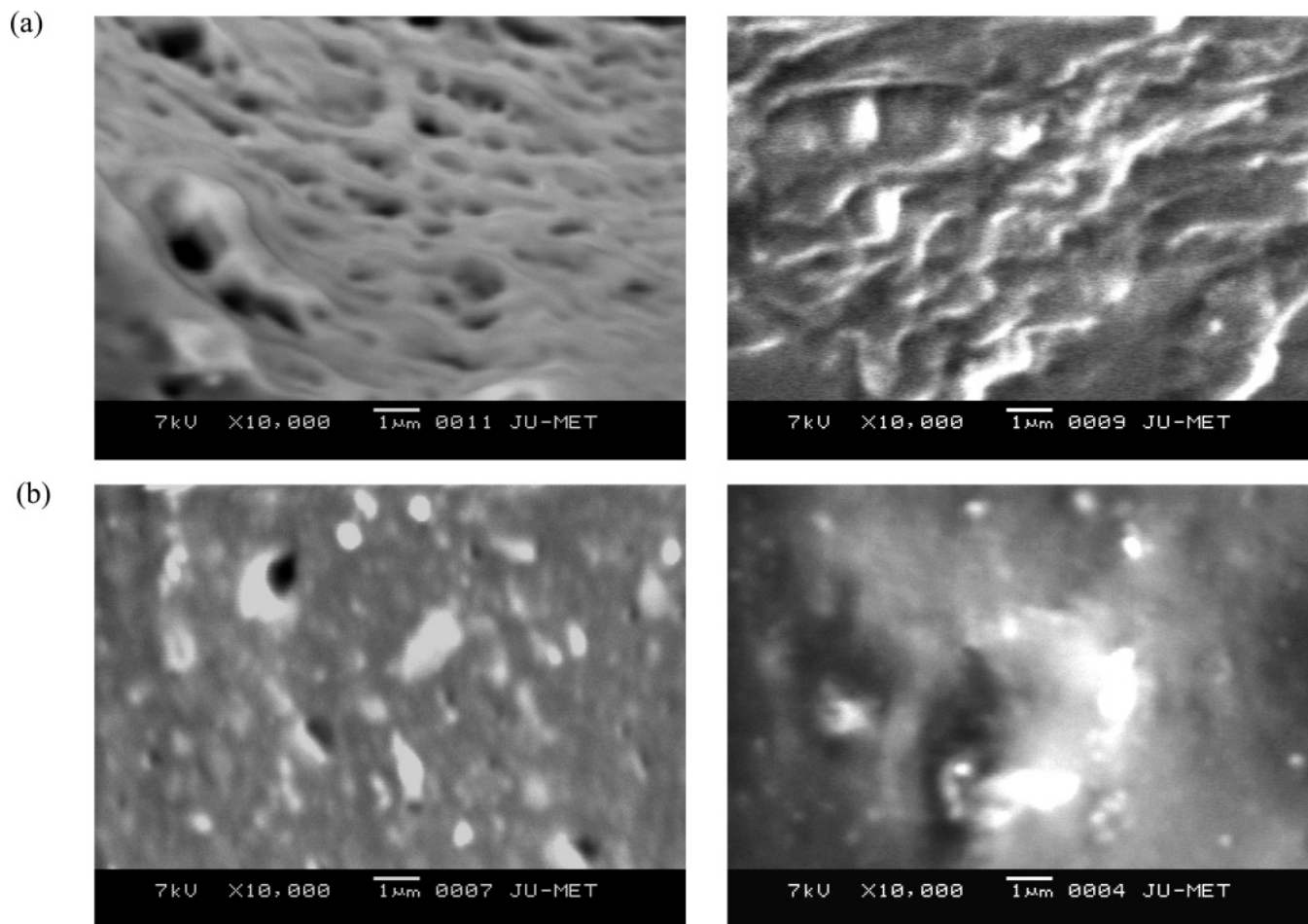
Figure 10. SEM picture of (a) solvent cast and (b) melt-cooled PNCs for PNC1 and PNC5, respectively.

the interchain exciton transfer in the solvent cast PNCs. But the absence of network structure in the melt-cooled PNCs causes the intrachain energy transfer, resulting in increased photoluminescence emission. Also, in the solvent cast PNCs, the clay tactoids are mostly in the exfoliated state (except PNC5),[11] and the exciton beam path is therefore not much increased as beam reflection is lesser due to different directional disposition of the clay tactoids. Also, the side chains in the melt-cooled PNCs are in mesomorphic arrangement whereas those in the solvent cast film are in crystalline order. The former may also be a cause for the red shift of photoluminescence. Thus, by changing the concentration of clay and applying a different procedure of PNC preparation, both emitted color and quantum yield of photoluminescence can be tailored.

H. dc Conductivity. The dc conductivity of the melt-cooled PNCs measured by the four-probe method at room temperature is presented in Table 3. From the table, it is apparent that the conductivity of undoped samples showed a 1 order decrease of conductivity in the PNCs compared with that of P3HT. It may be explained from the blue shift of the $\pi-\pi^*$ absorption peak of the P3HT chain in the UV−vis spectra (Figure 8). The conductivity of melt-cooled undoped PNCs are comparable to that of solvent cast PNCs,[11] but in the doped samples, it is lower. In the PNCs, the band gap between valence band and the conduction band increased as conjugation length decreases due to an increased rigidity imposed by the cohesive force of the clay tactoids. However, the conductivity is almost invariant in the PNCs with an increase in clay concentration, as the blue shift in the UV−vis spectra of PNCs is almost the same from the pure P3HT. The reason for the 2−3 order increase in
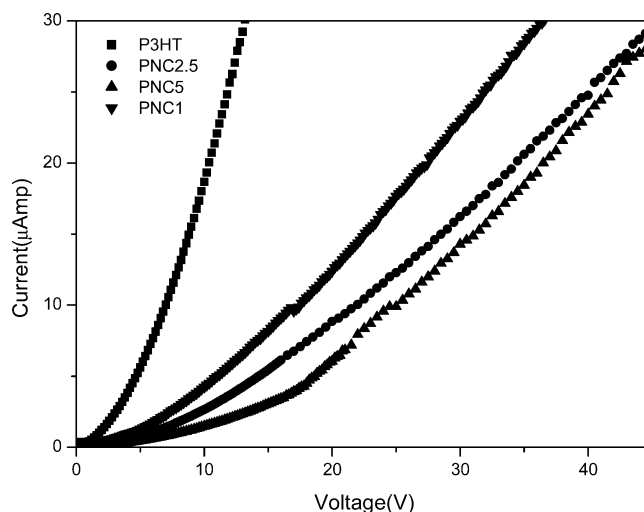
Figure 11. *I−V* characteristic of different melt-cooled P3HT and its PNCs.

conductivity in the doped sate for solvent cast films compared with melt-cooled PNCs is not known. Probably, the more ordered structure of solvent cast samples in the doped state increases the carrier mobility more compared to that in the melt-cooled PNCs. In Figure 11, the *I−V* characteristic curves of melt-cooled P3HT and PNCs are compared. The *I−V* curves of Figure 11 characterize the semiconducting behavior of all the samples, and with the addition of clay, the insulating behavior gradually develops. As, for example, for the flow of the same current (e.g., 30 μA) through the PNCs, it requires

Poly(3-hexyl thiophene)−Montmorillonite

J. Phys. Chem. B, Vol. 110, No. 4, 2006 **1631**

four times the voltage than pure P3HT. This means that the clay tactoids hinder the flow of the charge carriers as they act as a barrier between the polymer chains. The charge carrier therefore becomes confined in the quantum-well-like structure, and the probability of the formation of excitons by a recombination process would increase. So, electroluminescence of the samples would dramatically increase and will be addressed in future.

Conclusions

The melt-cooled PNCs of P3HT show different properties than solvent cast PNCs. A third-order hierarchy exists in the structure of all the melt-cooled PNCs, which showed mainly intercalated structures. Here, the P3HT side chain has liquid crystalline morphology, followed by the interchain lamella of P3HT, and finally it is intercalated by clay tactoids. The WAXS data supports the formation of an intercalated structure and liquid crystalline morphology. The TGA data showed that the degradation temperature of P3HT decreases in the PNCs, which is in sharp contrast with that of solvent cast samples. The easier degradation of liquid crystalline polymorph than that of a crystalline polymorph has been attributed to such a different behavior. The melting points of the PNCs increased by 2−3 °C from that of pure P3HT. The T_g and T_β values of the PNCs have increased from those of the P3HT indicating clay tactoids hinder the various bond movements. The storage modulus showed a dramatic increase in the melt-cooled PNCs, but it is smaller than that of solvent cast PNCs. The UV−vis spectra showed a blue shift whereas the photoluminescence spectra show a red shift with increasing clay concentration. The former has been attributed to the induced rigidity of P3HT chains by clay tactoids whereas the latter is explained from the structural polydispersity and liquid crystalline nature of the material. The isolation of polymer chains by the clay tactoids also results in an increased luminescence efficiency. The conductivity of PNCs decreased due to an increased band gap for induced rigidity by clay tactoids, and the $I−V$ characteristic curves concludes semiconducting behavior of the material.

References and Notes

(1) Giannelis, E. P.; Krishnamoorti, R.; Manias, E. *Adv. Polym. Sci.* **1999**, *138*, 107.

(2) Vaia, R. A.; Krishnamoorti, R. In *Polymer Nanocomposites: Synthesis Characterization and Modeling*; Krishnamoorti, R., Vaia, R. A., Eds.; American Chemical Society: Washington, DC, 2001; p 1.

(3) Okamoto, M.; Morita, S.; Kim, Y. H.; Kotaka, T.; Tateyama, H. *Polymer* **2001**, *42*, 1201.

(4) Maiti, P.; Nam, P. H.; Okamoto, M.; Hasegawa, N.; Usuki, A. *Macromolecules* **2002**, *35*, 2042.

(5) Fornes, T. D.; Yoon, P. J.; Keskkula, H.; Paul, D. R. *Polymer* **2001,** *42*, 9929.

(6) Park, J. H.; Jana, S. C. *Macromolecules* **2003**, *36*, 2758.

(7) Alexandre, M.; Dubois, P. *Mater. Sci. Eng. Rev.* **2000**, *R28* (1−2), 1.

(8) Lee, T.-W.; Park, O O.; Kim, J.-J.; Hong, J.-M.; Kim, Y. C. *Chem. Mater.* **2001**, *13*, 2217.

(9) Kim, B.-H.; Jung, J.-H.; Hong, S.-H.; Joo, J.; Epstein, A. J.; Mizoguchi, K.; Kim, J. W.; Choi, H. J. *Macromolecules* **2002**, *35*, 1419.

(10) Goddard, Y. A.; Vold, R. L.; Hoatson, G. L. *Macromolecules* **2003**, *36*, 1162.

(11) Kuila, B. K.; Nandi, A. K. *Macromolecules* **2004**, *37*, 8577.

(12) do Nascimento, G. M.; Constantino, V. R.L.; Temperini, M. L. A. *Macromolecules* **2002**, *35*, 7535.

(13) Lee, D.; Char, K.; Lee, S. W.; Park, Y. W. *J. Mater. Chem.* **2003**, *13*, 2942.

(14) Kim, B. H.; Jung, J. H.; Kim, J. W.; Choi, H. J.; Joo, J. *Synth. Met.* **2001**, *117*, 115.

(15) Wu, Q.; Xue, Z.; Qi, Z.; Wang, F. *Polymer* **2000**, *41,* 2029.

(16) Liu, Y.-C.; Tsai, C.-J. *Chem. Mater.* **2003**, *15*, 320.

(17) McCullough, R. D.; Ewbank, P. C. In *Handbook of Conducting Polymers*, 2nd ed.; Skotheim, T. A., Elsebaumer, R. L., Reynolds, J. R., Eds.; Marcel Dekker: New York, 1998; p 225.

(18) Prosa, T. J.; Winokur, M. J.; McCullough, R. D. *Macromolecules* **1996**, *29*, 3654.

(19) Meille, S. V.; Romita, V.; Caronna, T.; Lovinger, A. J.; Catellani, M.; Belobrzeckaja, L. *Macromolecules* **1997**, *30*, 7898.

(20) Bolognesi, A.; Porzio, W.; Zhuo, G.; Ezquerra, T. *Eur. Polym. J.* **1996**, *32*, 1097.

(21) Amou, S.; Haba, O.; Shirato, K.; Hayakawa, T.; Ueda, M.; Takeuchi, K.; Asai, M. *J. Polym. Sci., Part A: Polym. Chem.* **1999**, *37*, 1943.

(22) Yeh, J.-M.; Liou, S.-J.; Lin, C.-Y.; Cheng, C.-Y.; Chang, Y.-W.; Lee, K.-R. *Chem. Mater.* **2002**, *14*, 154.

(23) Frommer, J. E.; Chance, R. R. In *Encyclopedia of polymer science & engineering,* 2nd ed.; Mark, H. F., Bikales, N. M., Overberger, C. G., Menges, G., Eds.; John Wiley & Sons: New York, 1986; Vol. 5, p 473.

(24) Gajewski, K. E.; Gilberr, M. H. In *Advances in Molecular Modelling*; Liotta, D., Ed.; JAI Press: Greenerick, CT, 1990; Vol. 2.

(25) Darder, M.; Coalilla, M.; Ruiz-Hitzky, E. *Chem. Mater.* **2003**, *15*, 3774.

(26) Chen, T.-A.; Wu, X.; Rieke, R. D. *J. Am. Chem. Soc*. **1995**, *117*, 233.

(27) Yeh, J.-M.; Liou, S.-J.; Lai, C.-Y.; Wu, P.-C.; Tsai, T.-Y. *Chem. Mater.* **2001**, *13*, 1131.

(28) Malik, S.; Nandi, A. K. *J. Polym. Sci., Part B: Polym. Phys.* **2002**, *40*, 2073.

(29) Mandelkern, L. In *Comprehensive Polymer Science*; Allen, G., Ed.; Pergamon Press: Oxford, U.K., 1989; Vol. 2, p 363.

(30) Ferry, J. D. *Viscoelastive properties of polymers*; John Wiley and Sons: New York, 1961.

(31) Kovacs, A. J. *Adv. Polym. Sci.* **1963**, *3*, 394.

(32) Nandi, A. K.; Mandal, B. M.; Bhattachariyya, S. N.; Roy, S. K. *Polym. Commun.* **1986**, *27*, 151.

(33) Liu, Y.; Xu, Y.; Zhu, D. *Macromol. Chem. Phys.* **2001**, *202*, 1010.

(34) Malik, S.; Batabyal, S. K.; Basu, C.; Nandi, A. K. *J. Mater. Sci. Lett.* **2003**, *22*, 1113.

(35) Rughooputh, S. D. D. V.; Hotta, S.; Heeger, A. J.; Wudl, F. *J. Polym. Sci., Part B: Polym. Phys.* **1987**, *25*, 1071.

(36) Nguyen, T.-Q.; Wu, J.; Doan, V.; Schwartz, B. J.; Tolbert, S. H. *Science* **2000**, *288,* 652.

(37) Chen, S. H.; Su, A. C.; Chang, C. S.; Chen, H. L.; Ho, D. L.; Tsao, C. S.; Peng, K. Y.; Chen, S. A. *Langmuir* **2004**, *20*, 8909.

(38) Rothberg, L. J.; Bao, Z. *J. Phys.: Condens. Matter* **2002**, *14*, 12261.